

Thermal performance analysis of a solar energy storage unit encapsulated with HITEC salt/copper foam/nanoparticles composite

Xin Xiao^{1, 2*}, Hongwei Jia³, Dongsheng Wen¹, Xudong Zhao²

¹School of Chemical and Process Engineering, University of Leeds, Leeds LS2 9JT,
UK

²Energy and Environment Institute, University of Hull, Hull HU6 7RX, UK

³School of Environmental Science and Engineering, Donghua University, Shanghai
201620, China

Abstract

HITEC salt (40 wt. % NaNO₂, 7 wt. % NaNO₃, 53 wt. % KNO₃) with a melting temperature of about 142 °C is a typical phase change material (PCM) for solar energy storage. Both aluminum oxide (Al₂O₃) nanopowder and metal foam were used to enhance pure HITEC salt, so as to retrieve the limitation of composite PCMs with single enhancement. The morphologies and thermo-physical properties of the composites were firstly characterized with Scanning Electron Microscope, Fourier-transform Infrared spectroscopy and Differential Scanning Calorimeter, respectively. A pilot test rig with a heater of 380 W located in the inner pipe was built, which was encapsulated with HITEC salt, nano-salt (HITEC salt seeded with 2 wt. % Al₂O₃ nanopowder) and salt/copper foam composite seeded with 2 wt. % Al₂O₃ nanopowder as storage media. Then heat storage and retrieval tests of the energy

* Corresponding author.

Email address: xiaoxin2010@alumni.sjtu.edu.cn, x.xiao@hull.ac.uk

storage system were conducted both for pure HITEC salt and composite PCMs at various heating temperatures. The temperature evolutions and distributions of the PCMs at different locations were measured, including radial, angular, and axial locations, and the energy and volumetric mean powers during heat storage/retrieval processes were calculated subsequently. The results show that metal foam is generally compatible with the nano-salt. The maximum deviation of the melting/freezing phase change temperatures of the nano-salt/copper foam composite is 3.54 °C, whereas that of the nano-salt/nickel foam composite is 3.80 °C. The specific heats of the nano-salt are apparently enhanced with the addition of Al₂O₃ nanopowder both in solid and liquid states. The system encapsulated with the nano-salt/copper foam composite can be considerably enhanced, e.g. the time-duration of heat storage process at the heating temperature of 160 °C can be reduced by about 58.5%, compared to that of pure salt. The volumetric mean power of heat storage for the nano-salt/copper foam composite at the heating temperature of 180 °C increases to 109.32 kW/m³, compared with 53.01 kW/m³ of pure HITEC salt. The information will be helpful for solar system design, construction and application using molten salt for solar energy storage.

Keywords: HITEC salt; aluminum oxide nanopowder; metal foam; thermal characterization; heat storage/retrieval

Nomenclature

c_p specific heat, kJ/(kg K)

d	diameter, mm
E	energy, kJ/kg
JF	comprehensive performance coefficient
m	mass, kg
\bar{P}	mean power, kW
\bar{P}_v	volumetric mean power, kW/m ³
T	temperature, °C
t	time, s
V	volume, m ³
z	position of thermocouple, mm

Subscripts

c	charging
d	discharging
i	inner
o	outer
PCM	phase change material

1

2 **1. Introduction**

3 The huge consumption of fossil energy has brought about energy crisis and
4 environmental issues. The applications of renewable energy are keys to developing
5 energy-saving and clean energy technologies [1-4]. The direct usage of solar energy as

1 one of the renewable energy is attracting attention recently, and a large amount of
2 research has been carried out regarding the high-efficiency usage of solar thermal
3 energy in heating and cooling [5-6]. Phase change materials (PCMs) are proposed as a
4 principal way to store the thermal energy regarding the intermittent of solar energy [7],
5 which is named latent thermal energy storage (LTES) and can stabilize the system.

6 Nitrate salts as PCMs have been widely used in the medium temperature range
7 (100~300 °C) of solar energy application [8-9]. However, the main drawbacks of pure
8 salts are the low thermal conductivity and specific heat. Many techniques have
9 addressed the issues of pure salts, including extended fins, macro- and
10 micro-encapsulation of the PCMs, addition of high-conductivity materials, and
11 impregnating the PCMs into highly conductive porous structures [8-11]. Metal foam
12 with good mechanical and thermal properties can be used as thermal spreader in pure
13 PCMs, which shows attractive heat transfer performance. A number of studies extensively
14 investigated the thermo-physical properties and system performances relating to metal
15 foam composites [12-16]. Zhao et al. [13] experimentally and numerically studied the heat
16 transfer performance enhancement by embedding metal foam in paraffin. It can be seen
17 that the overall heat transfer rates were enhanced by 5~20 times in the solid region and
18 3~10 times in the liquid region during melting process, respectively. Zhang et al. [14]
19 experimentally and numerically studied the heat transfer performance of a LTES unit
20 encapsulated with the salt/metal foam composite. The results indicated that the
21 time-durations of heat retrieval process for the salt/copper foam composite and

1 salt/nickel foam composite showed 28.8% and 19.3% reduction, respectively, when the
2 cooling temperature was 30 °C. Zhang et al. [15] experimentally and theoretically studied
3 the performance of an AISI 321 tube encapsulated with NaNO₃/KNO₃, whereas metallic
4 foam and metallic sponge were used to enhance the effective thermal conductivity of the
5 PCM. Yang et al. [16] numerically studied the melting characteristics of a
6 shell-and-tube LTES unit enhanced with metal foam, and the influences of metal foam
7 location and porosity on the thermal performance of the LTES unit were analyzed
8 extensively. It was found that the porosity of metal foam could affect the temperature
9 field of PCMs, and the melting time can be maximally reduced by 88.55% together with
10 *j*-f factor increased by 5186.91% in comparison with a smooth tube [16].

11 Nanoparticle has a high particle surface energy due to its large specific surface area,
12 and it can make slight improvement in thermal conductivity and lead to keep and increase
13 the specific heat of pure PCM [17-25]. The nanocomposites synthesized with PCMs and
14 nanoparticles have been studied extensively, both for thermo-physical properties and
15 system performances. Navarrete et al. [18] characterized solar salt nano-encapsulated
16 with Al-Cu alloy layer and pointed out that the total energy stored of the system can be
17 increased owing to contribution of the latent heat storage of the nano-encapsulated
18 PCM, e.g., the thermal storage capacity can be increased by 17.8% when the PCM was
19 nanoencapsulated with an aluminium oxide layer. Mayilvelnathan and Arasu [19]
20 prepared and studied the erythritol/graphene composite PCM. It was found that the
21 thermal conductivity could be increased to 1.122 W/(m K) with the addition of 1 wt. %

1 graphene nanoparticles. Zhang et al. [20] synthesized the micro-capsuled PCM
2 (mePCM) with binary carbonate salt, and the mePCM showed an enhanced effective
3 heat capacity of 1.34-fold compared to the best commercialized product in a CSP
4 system. Chieruzzi et al. [21] prepared and characterized the nanofluids with binary salt
5 ($\text{NaNO}_3\text{-KNO}_3$ with 60:40 ratio) and 1.0 wt. % $\text{SiO}_2/\text{Al}_2\text{O}_3$ (silicon dioxide/aluminium
6 oxide) nanoparticles. The results showed that the nanoparticles induced a maximum
7 increase of 52.1% in solid phase and 18.6% in liquid phase of specific heat. Li et al.
8 [22] prepared the binary molten salt nanofluids with nitrates and SiO_2 nanoparticles,
9 where the nanoparticles with different diameters and mass fractions were investigated.
10 It was found that the specific heat was about 17.8 % higher, while the average thermal
11 conductivity was 20.2% higher, in comparison with those of pure molten salt. Liu and
12 Yang [23] investigated the specific heat and latent heat of eutectic hydrate salt doped
13 with TiO_2 nanoparticles. It showed that the specific heats increased by 83.5% in solid
14 state and 15.1% in liquid state with the addition of 0.3% TiO_2 , while the latent heat was
15 up to 6.4%. Song et al. [24] experimentally investigated the effects of the mixing time
16 and stirring rate of preparation of molten-salt nanofluids on the specific heats of
17 quaternary nitrate dispersed with SiO_2 nanoparticles. It showed that the specific heats of
18 the molten-salt nanofluids could be enhanced due to the formation of nanostructures.
19 Ho and Pan [25] investigated the influences of Al_2O_3 nanoparticle concentrations on the
20 heat transfer characteristics of nano-HITEC salt flowed in a circular tube. Both the
21 mean and local Nusselt numbers exhibited significant enhancement with the addition of

1 Al_2O_3 nanopowder, e.g. a maximum enhancement of the mean Nusselt number could be
2 up to 11.6% when the concentration of Al_2O_3 nanoparticles was 0.25 wt. %. However,
3 the thermal conductivities of most nanocomposites are below 1.0 W/(m K).

4 Meanwhile, it has been proven that the combination of metal foam and nanoparticles
5 is a promising solution to enhance the thermo-physical properties of pure salt or other
6 [26-28]. Thus it is of great importance to incorporate high-conductivity nanoparticles
7 into metal foam, so as to make the attractive enhancement of pure PCMs. However, it
8 can be seen from the aforementioned research that the thermo-physical properties of
9 nano-salt/copper foam composite was seldom investigated. Besides the thermo-physical
10 properties of the nano-salt at a small scale, it is indispensable to investigate the thermal
11 response of the nano-salt in an energy storage unit. None of the previous studies
12 reported heat transfer investigations of nano-salt with and without porous medium in a
13 large scale rig setup, while the heat transfer performance of a storage medium (nano-salt
14 with porous medium) is interesting and needs to be revealed. In the present study, in
15 order to store the thermal energy in the temperature range of 100~200 °C for electricity
16 generation, common HITEC salt (40 wt. % NaNO_2 , 7 wt. % NaNO_3 , 53 wt. % KNO_3)
17 as a ternary nitrate/nitrite mixture was used as the base material, and Al_2O_3 nanopowder
18 and metal foam were applied to enhance thermo-physical properties of pure HITEC salt.
19 The morphologies and thermal characteristics of the composites were firstly
20 characterized with Scanning Electron Microscope (SEM), Fourier-transform Infrared
21 (FT-IR) spectroscopy and Differential Scanning Calorimeter (DSC), respectively. A

pilot experimental rig with a heater located in the inner pipe was built, which encapsulated HITEC salt, nano-salt (HITEC salt seeded with 2 wt. % Al_2O_3) and nano-salt/copper foam composite as storage media. Then heat storage and retrieval tests of the LTES unit were conducted both for pure salt and composite PCMs, while the temperature distributions of the PCMs at different locations were measured, including radial, angular, and axial locations. The heat transfer characteristics together with the volumetric mean powers of the LTES unit were extensively revealed. The findings from the present study can broaden the application of nano-salt with and without porous medium. The accurate data of the thermo-physical properties of the nano-salt/metal foam composite PCMs play key roles for designing and modeling the LTES system. The output power and heat storage/retrieval rates of the LTES system can be improved greatly with the composite PCMs, and therefore the energy efficiency of the LTES system increases.

2. Materials preparation and experimental set-up

2.1 Synthesis of composite PCMs

NaNO_2 (Alfa Aesar, UK), NaNO_3 (Honeywell Fluka, UK) and KNO_3 (Acros Organics, UK), all with 99.0 % purity were used as the base materials in the present study. They were uniformly mixed with the mass ratios of 40:7:53 to form HITEC salt. Al_2O_3 nanopowder (40-80 nm APS, Nanostructured & Amorphous Materials Inc., US) and metal foam (Kunshan Jiayisheng Electronics Co. Ltd., CN) with the porosity of

about 95.0% and pore size of 10 PPI (pores per inch) were used to enhance the thermo-physical properties of pure salt. The synthesized process of HITEC salt/metal foam composites seeded with Al_2O_3 nanopowder was shown in **Fig. 1**.

Pure HITEC salt was first dissolved into deionized water, and Al_2O_3 nanopowder with mass fraction of 1%, 2% or 3% was suspended in the solution, respectively, stirred and sonicated for 60 mins with an ultrasonicator (FB15057) under the power of 600 W and frequency of 37 kHz for good dispersion. Then nickel foam or copper foam was physically immersed in the solution filled in a stainless steel disc. Subsequently the solution after 10 mins sonication was heated in an eurotherm oven (Carbolite Sheffield, UK) at 200 °C to evaporate the water and ensure the impregnation. Finally the disc filled with salt/metal foam composites seeded with Al_2O_3 nanopowder was taken out and naturally cooled, which was done at an oven with 30 °C for 2 mins. The composite PCMs separated were removed and slightly polished with the abrasive paper to make the surface smooth.

2.2 Characterization of composite PCMs

Series characterizations of the properties of the composites were addressed subsequently, and three specimens of each type were tested to ensure the repetition and accuracy of the results. The morphologies of the composites were characterized by tabletop Microscope TM3030Plus (Hitachi High-Technology, Japan), while BSE (Backscattered Electrons) and EDX (Energy Dispersive X-ray Spectrometer) modes

1 were used. FT-IR Perkin Elmer device (Thermo Scientific, NICOLET iS10) was used
2 as the supplement of the component analysis, contributing to analyze the chemical
3 bonding, molecular structure and degradation effect of the specimens. During the
4 measurement of FT-IR, the specimens were subjected to infrared light and the
5 absorption and emission of wave length were monitored, where the covered wavelength
6 ranged from 400 cm^{-1} to 4000 cm^{-1} in the present study.

7 A Mettler-Toledo DSC (Mettler Toledo Ltd., Leicester, UK) was used to
8 characterize the phase change behaviours of the composites. The accuracy of
9 temperature measurement is within $\pm 0.02\text{ }^{\circ}\text{C}$, and the resolution of the furnace
10 temperature is within $\pm 0.00006\text{ }^{\circ}\text{C}$. All the specimens were slightly heated until they
11 reached $50\text{ }^{\circ}\text{C}$. Then they were subjected to melting–freezing cycles under the same test
12 conditions with the heating and cooling rates of $5\text{ }^{\circ}\text{C}/\text{min}$ within a temperature range
13 from $50\text{ }^{\circ}\text{C}$ to $200\text{ }^{\circ}\text{C}$. Two melting-freezing cycles were conducted and the average
14 values were used to characterize the phase change temperatures and latent heats of
15 HITEC salt, salt/ Al_2O_3 nanopowder nanocomposite (nano-salt), salt/metal foam
16 composite and salt/metal foam composite seeded with Al_2O_3 nanopowder. In addition,
17 the specific heats were measured and calculated with the multiple curving methods [21,
18 29], including empty crucible curve, sapphire curve, and specimen curve. The crucibles
19 were subjected to the same heating procedure, which was isothermal at $100\text{ }^{\circ}\text{C}$ for 10
20 min, heating from $100\text{ }^{\circ}\text{C}$ to $300\text{ }^{\circ}\text{C}$ with the rate of $25.0\text{ }^{\circ}\text{C}/\text{min}$ and kept constant at
21 $300\text{ }^{\circ}\text{C}$ for 10 min. Then the specific heats of the specimen were calculated in

comparison with those of sapphire already known.

2.3 Heat storage/retrieval tests of pure salt and composite PCMs

2.3.1 Experimental rig and procedure

Fig. 2 shows the schematic of the LTES unit, which is with a diameter of 95.0 mm and a height of 300.0 mm. It can be seen from **Fig. 2(a)** that a cartridge heater, which worked as heat source, was located in the inner pipe made of the stainless steel with a diameter of 25.0 mm, while the surrounding was encapsulated with pure salt or composite PCMs. The power of the heater was provided via a control system using LabVIEW software, with a maximum power of 380 W. Various thermocouples of type *K* with a diameter of 3.0 mm were inserted at different locations inside the PCMs region, so as to measure the temperature distributions at radial, angular, and axial locations, as shown in **Fig. 2(b)**. The thermocouples labelled with *TD2*, *TD3*, *TD4* and *TD5* were located in the middle axial positions at $z=150$ mm. Those thermocouples were different at radial direction, and the distances from the centre of the heater are 22.5 mm, 27.5 mm, 32.5 mm, 37.5 mm, respectively. Other thermocouples labelled with *T3*, *T4* and *T5* were located at $z=125$ mm, and *T6* in the farthest radial direction were at the deepest point. During the tests, *T4*, *T4'*, *T4''* and *T4'''* located in four angular directions were used to check the homogenous heat transfer within the PCMs. In addition, a power meter was used to measure the power consumption as a reference in each experiment. The test rig was covered with multilayer thermal insulation and

1 radiant shielding (aluminium fibre) materials, so as to reduce the heat loss of the LTES
2 unit. Because of the safety consideration, a safety pressure relief valve was added to
3 ensure no pressure accumulated inside the LTES unit.

4 The LTES unit was encapsulated with three types of PCMs, including HITEC salt,
5 salt/2 wt. % Al_2O_3 nanopowder nanocomposite (nano-salt), salt/copper foam composite
6 seeded with Al_2O_3 nanopowder, respectively. Because salt and nano-salt were filled in
7 powder state, only 90.0% of the volume of the LTES unit was filled and the left space
8 was used for adapting the thermal expansion of about 7% for the PCM [30]. The
9 HITEC salt powder filled in three cases were 2300 g, 2250g and 2100 g, respectively,
10 with the addition of Al_2O_3 nanopowder and copper foam in the two latter cases. Thus
11 the mass of the nano-salt and nano-salt/copper foam composite were 2295 g and 2780 g,
12 respectively.

13 The whole LTES unit was at a surrounding temperature of about 10~20 °C initially,
14 then the heat storage tests were conducted. The heating temperatures were set as 160 °C,
15 180 °C and 200 °C for HITEC salt and its composites, respectively, so as to investigate
16 the performances of the LTES unit at various conditions. The heat retrieval tests were
17 started subsequently after the main unit approximately reached the heating temperatures.
18 During heat retrieval process, the whole unit was cooled down naturally at the
19 surrounding temperature of about 13~18 °C. Although the test rig was located in the
20 ventilating cabine of the lab with air conditioning, the temperature of the ventilating
21 cabine still fluctuated, which caused the variation of the surrounding temperature. The

1 temperature evolutions of all thermocouples were instantly recorded with the time
 2 interval of 1.4 s once the tests started, where the interval were determined by a program
 3 in Labview software. A first thermal cycle was made to remove the air in salt powder,
 4 and the temperature evolutions during heat storage/retrieval processes presented in the
 5 present study were obtained under the second thermal cycle.

6

7 **2.3.2 Energy and volumetric mean power of the LTES unit**

8 The specific heats of pure salt and composite PCMs can be considered
 9 approximately as a function of the temperature in the entire temperature range [31]. The
 10 latent heat accounting for the phase change process can be incorporated into the
 11 specific heat of the PCM, which is named apparent specific heat. In the present study,
 12 the energy absorbed by the LTES unit can be obtained with the summation of the latent
 13 and sensible energy stored by the PCMs. As a result, the apparent specific heat was
 14 used to calculate the energy based on the mass of the PCMs filled in the LTES unit.
 15 Then the energy and volumetric mean powers of the LTES unit during heat storage
 16 process were calculated as follows, respectively:

$$E_c = m_{PCM} \int_{30}^{T_{heating}} c_{p,PCM} dT \quad (1)$$



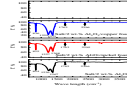
$$P_c = \frac{E_c}{t_c} \quad (2)$$

17 Where t_c is the time-duration of heat storage considered from 30 °C to the heating
 18 temperatures. The energy and volumetric mean powers of the LTES unit during heat

retrieval process were defined as follows, respectively:



(3)



(4)

where t_d is the time-duration of heat retrieval from the heating temperatures to the end temperatures. As the initial temperatures during heat retrieval were a little larger than the heating temperatures, t_d was adjusted to start from $T=T_{heating}$. In the present study, the end temperatures during heat retrieval were set as 50 °C, 60 °C and 70 °C, respectively, so as to get the insight of the optimal temperature difference between the final temperature and surrounding for the application.

2.3.3 Experimental uncertainty analysis

The thermocouples were pre-calibrated with the uncertainty of 0.5 °C, and the uncertainty of the position of the thermocouple was about 3.0 mm. The expanded uncertainty of the temperature evolutions can be obtained by the uncertainty propagation analysis, shown as below:

$$\frac{\delta T}{T} = \sqrt{\left(\frac{\delta T_{thermocouple}}{T_{thermocouple}}\right)^2 + \left(\frac{\delta z}{z}\right)^2} \quad (5)$$

Thus the maximum uncertainty for the temperature evolutions was determined to be 2.02%. Both the uncertainties of the weight and specific heat of the PCM were 0.5%, and the uncertainty of the time-duration was 1.0%. The overall uncertainty of the

volumetric mean power, mainly attributed to the uncertainties in weight and specific heat of PCM, temperature evolution and time-duration, was determined to be 2.36% with the following equation.

$$\frac{\delta \bar{P}}{\bar{P}} = \sqrt{\left(\frac{\delta m}{m}\right)^2 + \left(\frac{\delta c_p}{c_p}\right)^2 + \left(\frac{\delta T}{T}\right)^2 + \left(\frac{\delta t}{t}\right)^2} \quad (6)$$

3. Results and discussion

3.1 Morphologies of composite PCMs

Fig. 3 shows the SEM images of the salt/Al₂O₃ nanocomposite with and without metal foam. It can be seen from **Fig. 3(a)** that Al₂O₃ nanopowder can mix well with salt, with a granular appearance. The structural interaction with salt molecules can be generated as it is difficult to distinguish nanoparticle from salt. **Fig. 3(b)-(c)** show that the salt/Al₂O₃ nanocomposite is generally compatible with metal foam, where the impregnation ratio of the present sample can reach 90.0% [32]. The rugged surface in **Fig. 3(c)** is caused by the shrinkage of the salt during freezing, as the density of the salt in solid state is larger than that in liquid state [30]. The phenomenon is similar to the previous study of the paraffin/metal foam composites [32].

Fig. 4 shows the FT-IR analyses of HITEC salt and composite PCMs, where the Y-axis indicates the transmittance ratio of infrared light. It can be seen that the FT-IR absorption spectra are nearly the same for all the specimens, indicating that the existence of the physical bonding of Al₂O₃ nanopowder with nitrate molecule does not disturb the

chemical structure interaction for chemical stability. The peaks between 1200 cm^{-1} ~ 1400 cm^{-1} are slightly obvious with the addition of Al_2O_3 nanopowder and metal foam, indicating that the good bonding between Al_2O_3 nanopowder and nitrate molecule exists.

3.2 Phase change behavior of composite PCMs

The variations of the phase change temperatures of pure salt and composite PCMs were characterized with DSC, as shown in **Fig. 5**. The extrapolated onset melting temperatures of the salt/nickel foam and salt/copper foam composites shifts to 139.67°C and 139.56°C , respectively, from 138.67°C for pure HITEC salt. The deviated tendencies of the melting temperatures can be explained by the Clapeyron-Clausius equation, and the same phenomenon was reported in a previous study [32]. It seems that the slight increase of the phase change temperature can be attributed to the restriction of the metal skeleton on the volume expansion. On the contrary, the addition of Al_2O_3 nanopowder can slightly decrease the extrapolated onset melting temperature and increase the extrapolated onset freezing temperature of pure HITEC salt, e.g., the extrapolated onset melting temperature shifts from 138.67°C to 137.74°C , while the extrapolated onset freezing temperature shifts from 141.79°C to 144.98°C , compared with those of HITEC salt. The phenomenon of the early occurrence of phase change can be attributed to the good combination and dispersion performance of the PCM and nano-promoter [29, 33], as depicted in **Fig. 3(a)**. The combined effects of metal foam and Al_2O_3 nanopowder contribute to the variation of phase change temperature of the

1 salt/metal foam composite seeded with 2 wt. % Al_2O_3 nanopowder to some extent, and
2 the maximum deviation of the melting/freezing phase change temperatures of the
3 nano-salt/copper foam composite is 3.54 °C, whereas that of the nano-salt/nickel foam
4 composite is 3.80 °C.

5 **Fig. 6** shows the examples of the apparent specific heats of HITEC salt and
6 composite PCMs, which incorporated with latent heat. **Table 1** also lists the mean
7 specific heats of HITEC salt and composite PCMs. The specific heats in solid state
8 were calculated within the temperature range of 105~120 °C, while those in liquid state
9 were calculated in the temperature range of 180~280 °C. It can be seen that the specific
10 heats of the nano-salts are apparently enhanced with the addition of Al_2O_3 nanopowder
11 both in solid and liquid states, while those of the salt/metal foam composite PCMs
12 decrease, compared with that of pure HITEC salt. The maximum enhancement is about
13 12.1% in solid state, and 5.8% in liquid state with a nanopowder concentration of 2
14 wt. %. Therefore, in order to keep the heat storage capacity of the LTES unit, HITEC
15 salt/copper foam composite seeded with 2 wt. % Al_2O_3 nanopowder was used as the
16 storage medium in the following system tests.

18 **3.3 Performance enhancement with Al_2O_3 nanopowders and metal foam**

19 **3.3.1 Comparisons between pure salt and composite PCM**

20 **Fig. 7** shows the temperature evolutions and distributions of HITEC salt and
21 composite PCMs both for heat storage and retrieval processes. Because the

thermocouple of T_6 locates near the wall of the LTES unit, the temperature is lower than other thermocouples due to the heat loss from the lateral surface of the LTES unit, as shown in the pentagonal region of **Fig. 7**. It can be seen from **Fig. 7 (a-I)** that the temperature of T_3 increases more quickly than that of TD_3 , which is due to natural convection during melting. Based on the calculation with empirical correlation [31], it is found that the equivalent thermal conductivity is five times of pure salt considering natural convection. As shown in the rectangular region in **Fig. 7 (a-I)**, there are slightly difference among T_4 , T_4' , T_4'' and T_4''' , which could be attributed to the following reasons. On one hand, there might be several cavities caused by the shrinkage of salt during freezing, inducing the temperature difference during heat storage process while the salt is still in solid state. However, the temperatures of T_4 , T_4' , T_4'' and T_4''' are almost the same while the salt is in liquid state. On the other hand, the positions of the four thermocouples might not be at the radial and axial positions exactly which also slightly affect the comparisons among those test points. In general, the heat transfer seems homogenous at the same radial and axial positions. The heat retrieval process shown in **Fig. 7(b)** seems very slow, which is due to natural air cooling domination inducing large thermal resistance.

Fig. 8 shows the comparisons of temperature evolutions and distributions of HITEC salt and composite PCMs, whereas points T_3 , T_4 and T_5 are selected as the representative thermocouples. The temperature of point T_5 of HITEC salt increases more quickly than that of the nano-salt, as shown in **Fig. 8(a)**. The viscosity of the

nano-salt increased slightly with the addition of nanoparticles [34], which restricts natural convection to some extent accordingly. It can be seen from **Fig. 8(a)** that the time-durations of the nano-salt and nano-salt/copper foam composite for heat storage are considerably reduced, e.g., the charging times are 9422 s and 4606 s for the nano-salt and nano-salt/copper foam composite, indicating a reduction of the time-duration by 15.1% and 58.5%, respectively, compared with 11095 s for HITEC salt. The apparent enhancement is similar to the previous research [14-15]. However, the discharging times ($T_{end}=50\text{ }^{\circ}\text{C}$) are 35527 s, 42686 s and 41286 s for HITEC salt, nano-salt, nano-salt/copper foam composite, respectively. The phenomenon of slight improvement can be attributed to natural air cooling with large thermal resistance outside the LTES unit dominated the whole process, despite the enhancement of the thermo-physical properties of the nano-salt and nano-salt/copper foam composite. Due to the enhanced heat transfer, the LTES unit with the nano-salt and nano-salt/copper foam composite can reach the higher temperature after heat storage, inducing the larger time-duration of heat retrieval. In addition, due to the variation of the inner temperature of the ventilating cabine in the lab, the experiments of pure HITEC salt were conducted at the surrounding temperatures of about 13-15 $^{\circ}\text{C}$, and those of nano-salt and nano-salt/copper foam composite were conducted at the surrounding temperatures of about 16-18 $^{\circ}\text{C}$.

3.3.2 Different heating temperatures

Fig. 9 shows the temperature evolutions and distributions of HITEC salt/copper

foam composite seeded with 2 wt. % Al_2O_3 nanopowder at different heating temperatures. It can be seen from **Fig. 9(a)** that the higher heating temperature controlled can accelerate the melting process, e.g., the charging times are 4711 s and 3577 s at the heating temperatures of 180 °C and 200 °C, respectively. This is due to large temperature difference between the heater and PCMs leads to the enhanced heat transfer. **Fig. 9(b)** shows the temperature evolutions during heat retrieval process. The discharging times are about 44258 s and 46298 s when the starting temperatures are 180 °C and 200 °C, respectively. More energy can be stored with the higher heating temperature, which induces larger time-duration of heat retrieval subsequently as air cooling dominated the heat transfer process.

3.4 Energy and volumetric mean power for heat storage/retrieval

Latent and sensible enthalpy change were estimated according to the mass and apparent specific heats of the PCMs encapsulated in the LTES unit. Then the heat storage and retrieval powers were approximately calculated accordingly, based on the time-duration of heat storage and retrieval processes. The energy and volumetric mean powers of the LTES unit are listed in **Tables 2** and **3**, respectively. Because of the slight decrease of specific heat and large mass of the nano-salt/copper foam composite encapsulated in the LTES unit, the energy stored by the composite PCMs is slightly higher, as shown in **Table 2**.

The volumetric mean powers of heat storage in the LTES unit range from 36.54 to

1 157.91 kW/m³, based on different heating temperatures and PCMs. While the
2 volumetric mean powers of heat retrieval from the LTES unit are in the range of
3 8.66~11.93 kW/m³, 9.31~13.84 kW/m³ and 11.99~16.92 kW/m³ when the final
4 temperatures are 50 °C, 60 °C and 70 °C, respectively. It can be seen from **Table 3** and
5 **Fig. 10** that the mean powers of the LTES unit during heat storage process were
6 significantly improved with the application of the composite PCM, e.g., the mean
7 power for the nano-salt/copper foam composite at the heating temperature of 180 °C
8 increases to 109.32 kW/m³, compared with 53.01 kW/m³ of pure HITEC salt. However,
9 the mean powers during heat retrieval process are quite different. There are slight
10 difference among various PCMs, which is due to natural air cooling dominated the
11 whole process, inducing the large time-duration of heat retrieval process.

12 It can also be seen from Table 3 that the volumetric mean powers of heat retrieval
13 for the nano-salt/copper foam composite at the heating temperature of 160 °C are 10.05
14 kW/m³, 10.92 kW/m³ and 12.90 kW/m³ when the end temperatures are 50 °C, 60 °C and
15 70 °C, respectively. Because the time-duration decreases more apparently in
16 comparison with the reduction of released energy, the volumetric mean power of heat
17 retrieval increases when the end temperature changes from 50 °C to 70 °C. It can be
18 attributed to the reason that the heat transfer process becomes slow when the temperature
19 difference between the LTES unit and surrounding decreases. It should be noted that if the
20 high end temperature is considered, the usable energy will be reduced although the
21 volumetric power increases. As a result, the suitable end temperature should be

considered in real application. A LTES system can be constructed by aligning many such LTES units in a heat storage tank with or without heat transfer fluid. The heat transfer performance of such LTES unit presented is the fundamental information for performance evaluation of a LTES system, which can be very useful in the real application of nano-salt with and without porous medium.

5 Conclusions

HITEC salt/2 wt. % Al_2O_3 nanopowder (nano-salt) and salt/metal foam composite seeded with 2 wt. % Al_2O_3 nanopowder were synthesized, and the morphologies and thermal characteristics of the composites were extensively characterized. The heat storage and retrieval characteristics of a pilot test rig were experimentally investigated, which was encapsulated with pure HITEC salt, nano-salt and nano-salt/copper foam composite as storage media. The main conclusions can be drawn as follows:

- (1) Both Al_2O_3 nanopowder and metal foam can mix well with pure HITEC salt, the addition of Al_2O_3 nanopowder can slightly decrease the extrapolated onset melting temperature and increase the extrapolated onset freezing temperature of pure salt. The maximum deviation of the melting/freezing phase change temperatures of the nano-salt/copper foam composite is 3.54 °C, whereas that of the nano-salt/nickel foam composite is 3.80 °C. The specific heats of the nano-salts are apparently enhanced with the addition of Al_2O_3 nanopowder both in solid and liquid states.
- (2) The tests of the LTES unit indicate that both Al_2O_3 nanopowder and copper foam

1 can significantly improve the heat transfer of pure HITEC salt, e.g., the
2 time-duration of heat storage can be reduced by 15.1% and 58.5% for the nano-salt
3 and nano-salt/copper foam composite, respectively. But the time-durations of heat
4 retrieval process are seldom improved as the process is dominated by natural air
5 cooling. Furthermore, the higher heating temperature can accelerate the melting
6 process, while the heat retrieval process will be much slower as more energy stored
7 at higher heating temperature accordingly.

8 (3) The volumetric mean powers of the LTES unit during heat storage process were
9 significantly improved with the application of the composite PCM, e.g., the
10 volumetric mean power for HITEC salt/copper foam composite seeded with 2
11 wt. % Al_2O_3 nanopowder at the heating temperature of 180 °C increases to 109.32
12 kW/m^3 , compared with 53.01 kW/m^3 of pure HITEC salt. However, the volumetric
13 mean powers during heat retrieval process are quite different, and slight difference
14 among various PCMs exists.

15

16 **Acknowledgements**

17 This research is supported by European Union's Horizon 2020 Research and
18 Innovation Programme under Marie Skłodowska-Curie grant agreement of No.706788.

19 The authors also thank Dr. Afrah Awad with the help of building the test rig.

20

21 **Reference**

- 1 [1] Hulshof D, Jepma C, Mulder M. Performance of markets for European renewable
2 energy certificates. *Energy Policy* 2019; 128: 697–710.
- 3 [2] Hosseinzadeh M, Sardarabadi M, Passandideh-Fard M. Energy and exergy analysis
4 of nanofluid based photovoltaic thermal system integrated with phase change
5 material. *Energy* 2018; 147: 636–47.
- 6 [3] Kuik O, Branger F, Quirion P. Competitive advantage in the renewable energy
7 industry: Evidence from a gravity model. *Renew. Energy* 2019; 131: 472–81.
- 8 [4] Zhang C, Cui CL, Zhang Y, Yuan JQ, Luo YM, Gang WJ. A review of renewable
9 energy assessment methods in green building and green neighborhood rating
10 systems. *Energ. Buildings* 2019; 195: 68–81.
- 11 [5] Riahia S, Jovet Y, Saman WY, Belusko M, Bruno F. Sensible and latent heat
12 energy storage systems for concentrated solar power plants, exergy efficiency
13 comparison. *Sol. Energy* 2019; 180: 104–15.
- 14 [6] Zhang HL, Kong WB, Tan TW, Baeyens J. High-efficiency concentrated solar
15 power plants need appropriate materials for high-temperature heat capture,
16 conveying and storage. *Energy*, 2017; 139: 52–64.
- 17 [7] Dsilva Winfred Rufuss D, Rajkumar V, Suganthi L, Iniyan S. Studies
18 on latent heat energy storage (LHES) materials for solar desalination
19 application-focus on material properties, prioritization, selection and future
20 research potential. *Sol. Energy Mat. Sol. Cells* 2019; 189: 149–65.
- 21 [8] Piti F, Zhao CY, Caceres G. Thermo-mechanical analysis of ceramic encapsulated

1 phase-change-material (PCM) particles. *Energy Environ. Sci.*, 2011; 4: 2117–24.

2 [9] Pitié F, Zhao CY, Baeyens J, Degrevé J, Zhang HL. Circulating fluidized bed heat
3 recovery/storage and its potential to use coated phase-change-material (PCM)
4 particles. *Appl. Energy*, 2013; 109: 505–13.

5 [10]Zhang HL, Baeyens J, Caceres G, Degreve J, Lv YQ. Thermal energy storage:
6 Recent developments and practical aspects. *Prog. Energy Combust.*, 2016; 53:
7 1–40.

8 [11]Mahdi JM, Lohrasbi S, Nsofor EC. Hybrid heat transfer enhancement for
9 latent-heat thermal energy storage systems: A review. *Int. J Heat Mass Tran.* 2019;
10 137: 630–49.

11 [12]Xiao X, Zhang P, Li M. Effective thermal conductivity of open-cell metal foams
12 impregnated with pure paraffin for latent heat storage. *Int. J Therm. Sci.* 2014; 81:
13 94–105.

14 [13]Zhao CY, Lu W, Tian Y. Heat transfer enhancement for thermal energy storage
15 using metal foams embedded within phase change materials (PCMs). *Sol. Energy*
16 2010; 84: 1402–12.

17 [14]Zhang P, Xiao X, Meng ZN, Li M. Heat transfer characteristics of a molten-salt
18 thermal energy storage unit with and without heat transfer enhancement. *Appl.*
19 *Energy* 2015; 137: 758–72.

20 [15]Zhang HL, Baeyens J, Degrevé J, Cáceres G, Segal R, Pitié F. Latent heat storage
21 with tubular-encapsulated phase change materials (PCMs). *Energy*, 2014; 76:

1 66–72.

2 [16]Yang XH, Yu JB, Guo ZX, Jin LW, He YL. Role of porous metal foam on the heat
3 transfer enhancement for a thermal energy storage tube. *Appl. Energy* 2019; 239:
4 142–56.

5 [17]Myers PD, Alam TE, Kamal R, Goswami DY, Stefanakos E. Nitrate salts doped
6 with CuO nanoparticles for thermal energy storage with improved heat transfer.
7 *Appl. Energy* 2016; 165: 225–33.

8 [18]Navarrete N, Mondragon R, Wen DS, Navarro ME, Ding YL, Enrique Julia J.
9 Thermal energy storage of molten salt - based nanofluid containing
10 nano-encapsulated metal alloy phase change materials. *Energy* 2019; 167: 912–20.

11 [19]Mayilvelnathan V, Arasu AV. Characterisation and thermophysical properties of
12 graphene nanoparticles dispersed erythritol PCM for medium temperature thermal
13 energy storage applications. *Thermochimica Acta* 2019; 676: 94–103.

14 [20]Zhang HF, Shin DY, Santhanagopalan S. Microencapsulated binary carbonate salt
15 mixture in silica shell with enhanced effective heat capacity for high temperature
16 latent heat storage. *Renew. Energy* 2019; 134: 1156–62.

17 [21]Chieruzzi M, Cerritelli GF, Miliozzi A, Kenny JM, Torre L. Heat capacity of
18 nanofluids for solar energy storage produced by dispersing oxide nanoparticles in
19 nitrate salt mixture directly at high temperature. *Sol. Energy Mater. Sol. C.* 2017;
20 167: 60–9.

21 [22]Li Y, Chen X, Wu YT, Lu YW, Zhi RP, Wang X, Ma CF. Experimental study on

1 the effect of SiO₂ nanoparticle dispersion on the thermophysical properties of
2 binary nitrate molten salt. Sol. Energy 2019; 183: 776–81.

3 [23]Liu YS, Yang YZ. Investigation of specific heat and latent heat enhancement in
4 hydrate salt based TiO₂ nanofluid phase change material. Appl. Therm. Eng. 2017;
5 124: 533–8.

6 [24]Song WL, Lu YW, Wu YT, Ma CF. Effect of SiO₂ nanoparticles on specific heat
7 capacity of low-melting-point eutectic quaternary nitrate salt. Sol. Energy Mat. Sol.
8 C. 2018; 179: 66–71.

9 [25]Ho MX, Pan C. Experimental investigation of heat transfer performance of molten
10 HITEC salt flow with alumina nanoparticles. Int. J. Heat Mass Transf. 2017; 107:
11 1094–103.

12 [26]Xiao X, Wen DS. Investigation on thermo-physical properties of molten salt
13 enhanced with nanoparticle and copper foam. IEEE Xplore Digital Library 2018:
14 1445–9.

15 [27]Mahdi JM, Nsofor EC. Solidification enhancement in a triplex-tube latent heat
16 energy storage system using nanoparticles-metal foam combination. Energy 2017;
17 126: 501–12.

18 [28]Javaniyan Jouybari H, Saedodin S, Zamzamian A, Eshagh Nimvari M, Wongwises
19 S. Effects of porous material and nanoparticles on the thermal performance of a flat
20 plate solar collector: An experimental study. Renew. Energy 2017; 114: 1407–18.

21 [29]Xiao X, Zhang P. Morphologies and thermal characterization of paraffin/carbon

1 foam composite phase change material. Sol. Energy Mat. Sol. C., 2013; 117:
2 451–461.

3 [30]Siegel NP, Bradshaw RW, Cordaro JB, Kruizenga AM. Thermophysical property
4 measurement of nitrate salt heat transfer fluids. In: Proceedings of the ASME 2011
5 5th International Conference on Energy Sustainability, ES2011-54058; 2011. p.
6 1–8.

7 [31]Xiao X, Zhang P. Numerical and experimental study of heat transfer characteristics
8 of a shell-tube latent heat storage system: Part I – Charging process. Energy 2015;
9 79: 337–50.

10 [32]Xiao X, Zhang P, Li M. Preparation and thermal characterization of paraffin/metal
11 foam composite phase change material. Appl. Energy 2013; 112: 1357–66.

12 [33]Li M. A nano-graphite/paraffin phase change material with high thermal
13 conductivity. Applied Energy, 2013, 106: 25-30.

14 [34]Xiao X, Zhang G, Ding YL, Wen DS. Rheological characteristics of molten salt
15 seeded with Al₂O₃ nanopowder and graphene. Energies, 2019; 12: 467.

16

17

18

19

20

21

1 **Table 1** Specific heats of HITEC salt and composite PCMs

Specific heat (kJ/(kg·°C))	HITEC salt [26]	+Al ₂ O ₃ [26]			HITEC salt/nickel foam	HITEC salt/copper foam [26]	HITEC salt /2 wt. % Al ₂ O ₃ /nickel foam	HITEC salt /2 wt. % Al ₂ O ₃ /copper foam
		1 wt. %	2 wt. %	3 wt. %				
Solid state	1.40	1.57	1.57	1.54	1.18	1.32	1.39	1.42
Liquid state	1.56	1.64	1.65	1.63	1.23	1.50	1.41	1.55

2

3

4

5

6

7

8

9

10

11

12

13

14

15

16

17

18

1 **Table 2** Heat storage and retrieval energies for pure salt and composite PCMs

E (kJ)		Pure HITEC salt	Salt/2 wt. % Al_2O_3 nanopowder	Salt/copper foam composite seeded with 2 wt. % Al_2O_3 nanopowder
Heat storage	$T_{\text{initial}}=30\text{ }^\circ\text{C},$ $T_{\text{end}}=160\text{ }^\circ\text{C}$	722.06	736.55	828.14
	$T_{\text{initial}}=30\text{ }^\circ\text{C},$ $T_{\text{end}}=180\text{ }^\circ\text{C}$	803.17	814.22	917.41
	$T_{\text{initial}}=30\text{ }^\circ\text{C},$ $T_{\text{end}}=200\text{ }^\circ\text{C}$	875.58	890.19	1006.13
Heat retrieval	$T_{\text{initial}}=160\text{ }^\circ\text{C},$ $T_{\text{end}}=50\text{ }^\circ\text{C}$	652.04	658.35	739.45
	$T_{\text{initial}}=180\text{ }^\circ\text{C},$ $T_{\text{end}}=50\text{ }^\circ\text{C}$	733.14	736.02	828.72
	$T_{\text{initial}}=200\text{ }^\circ\text{C},$ $T_{\text{end}}=50\text{ }^\circ\text{C}$	805.56	811.99	917.44
	$T_{\text{initial}}=160\text{ }^\circ\text{C},$ $T_{\text{end}}=60\text{ }^\circ\text{C}$	617.04	621.03	696.84
	$T_{\text{initial}}=180\text{ }^\circ\text{C},$ $T_{\text{end}}=60\text{ }^\circ\text{C}$	698.27	697.02	784.04
	$T_{\text{initial}}=200\text{ }^\circ\text{C},$ $T_{\text{end}}=60\text{ }^\circ\text{C}$	770.55	774.39	874.34
	$T_{\text{initial}}=160\text{ }^\circ\text{C},$ $T_{\text{end}}=70\text{ }^\circ\text{C}$	582.01	581.93	652.49
	$T_{\text{initial}}=180\text{ }^\circ\text{C},$ $T_{\text{end}}=70\text{ }^\circ\text{C}$	663.26	657.92	739.70
	$T_{\text{initial}}=200\text{ }^\circ\text{C},$ $T_{\text{end}}=70\text{ }^\circ\text{C}$	735.54	735.29	829.99

2

3

4

5

1 **Table 3** Volumetric mean powers of heat storage and retrieval for pure salt and
2 composite PCMs

\bar{P}_V (kW/m ³)		Pure HITEC salt	Salt/2 wt.% Al ₂ O ₃ nanopowder	Salt/copper foam composite seeded with 2 wt.% Al ₂ O ₃ nanopowder
Volumetric mean power of heat storage	$T_{initial}=30\text{ }^{\circ}\text{C},$ $T_{end}=160\text{ }^{\circ}\text{C}$	36.54	43.89	100.94
	$T_{initial}=30\text{ }^{\circ}\text{C},$ $T_{end}=180\text{ }^{\circ}\text{C}$	53.01	66.63	109.32
	$T_{initial}=30\text{ }^{\circ}\text{C},$ $T_{end}=200\text{ }^{\circ}\text{C}$	81.84	96.09	157.91
Volumetric mean power of heat retrieval	$T_{initial}=160\text{ }^{\circ}\text{C},$ $T_{end}=50\text{ }^{\circ}\text{C}$	10.30	8.66	10.05
	$T_{initial}=180\text{ }^{\circ}\text{C},$ $T_{end}=50\text{ }^{\circ}\text{C}$	11.07	9.01	10.51
	$T_{initial}=200\text{ }^{\circ}\text{C},$ $T_{end}=50\text{ }^{\circ}\text{C}$	11.93	9.47	11.12
	$T_{initial}=160\text{ }^{\circ}\text{C},$ $T_{end}=60\text{ }^{\circ}\text{C}$	10.94	9.31	10.92
	$T_{initial}=180\text{ }^{\circ}\text{C},$ $T_{end}=60\text{ }^{\circ}\text{C}$	11.97	9.51	11.33
	$T_{initial}=200\text{ }^{\circ}\text{C},$ $T_{end}=60\text{ }^{\circ}\text{C}$	13.84	10.00	11.93
	$T_{initial}=160\text{ }^{\circ}\text{C},$ $T_{end}=70\text{ }^{\circ}\text{C}$	13.62	11.99	12.90
	$T_{initial}=180\text{ }^{\circ}\text{C},$ $T_{end}=70\text{ }^{\circ}\text{C}$	14.74	12.27	13.99
	$T_{initial}=200\text{ }^{\circ}\text{C},$ $T_{end}=70\text{ }^{\circ}\text{C}$	16.92	12.12	14.85

3

4

5

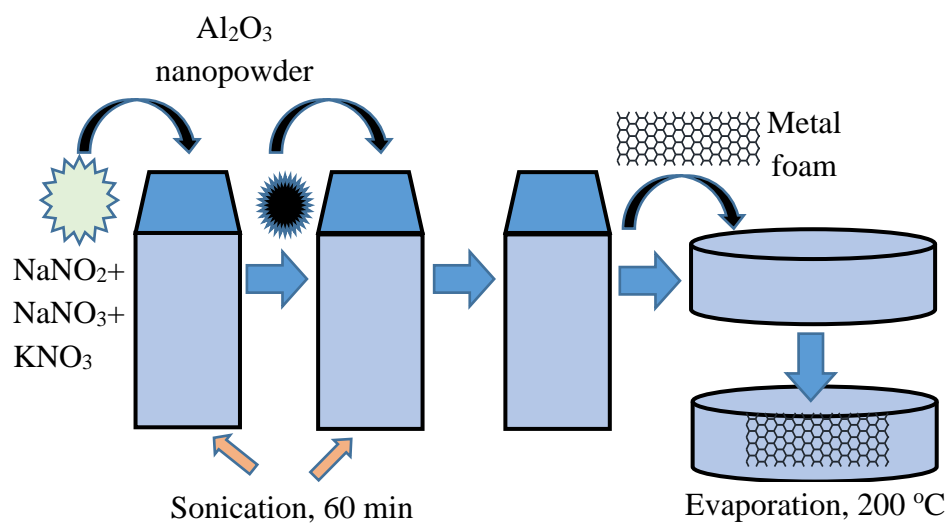


Fig. 1. Schematic of synthesis of salt/metal foam composites seeded with Al_2O_3

nanopowder. [26]

1
2
3
4
5
6
7
8
9
10
11
12
13
14
15

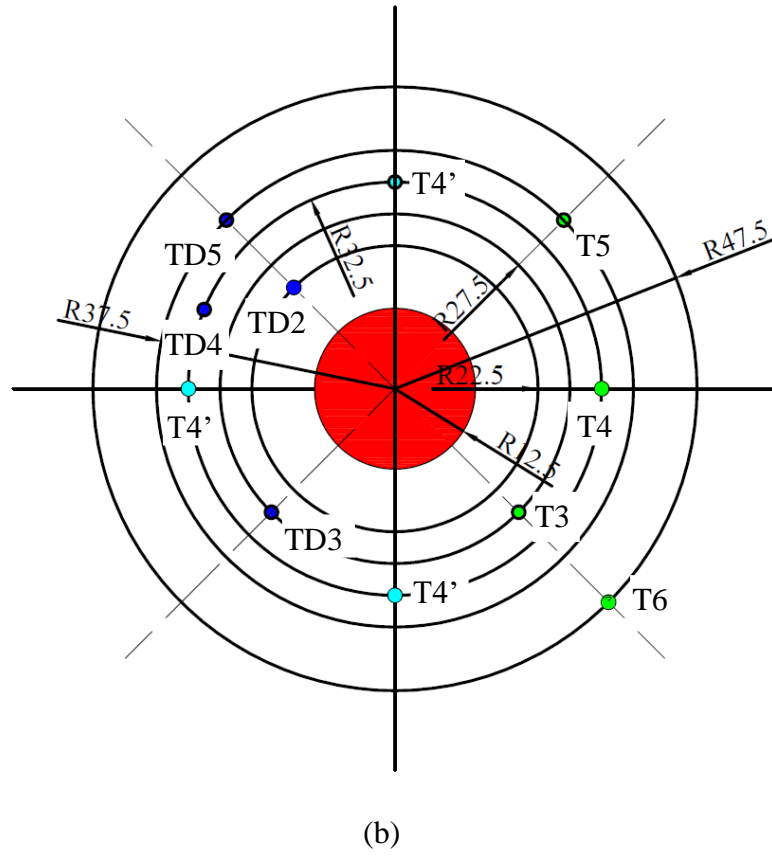
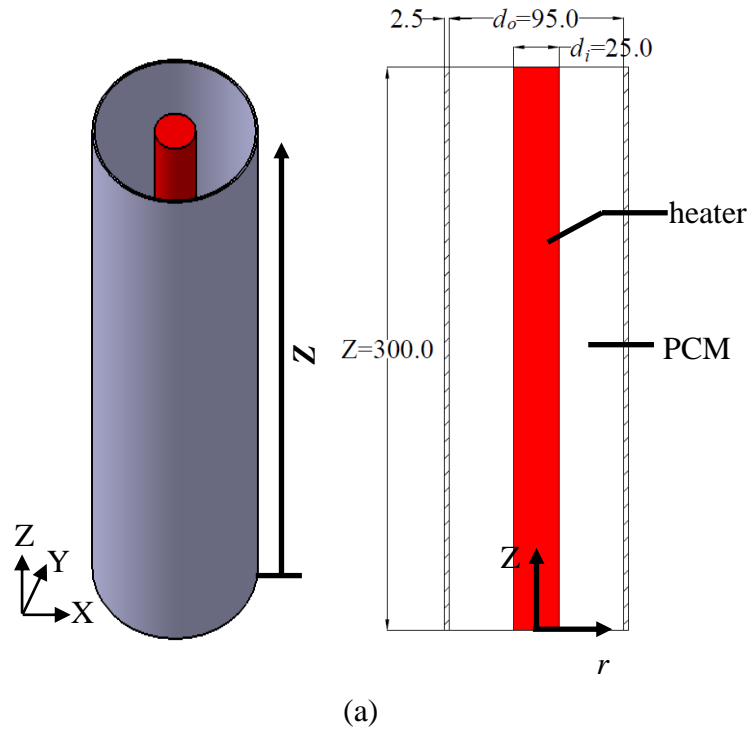
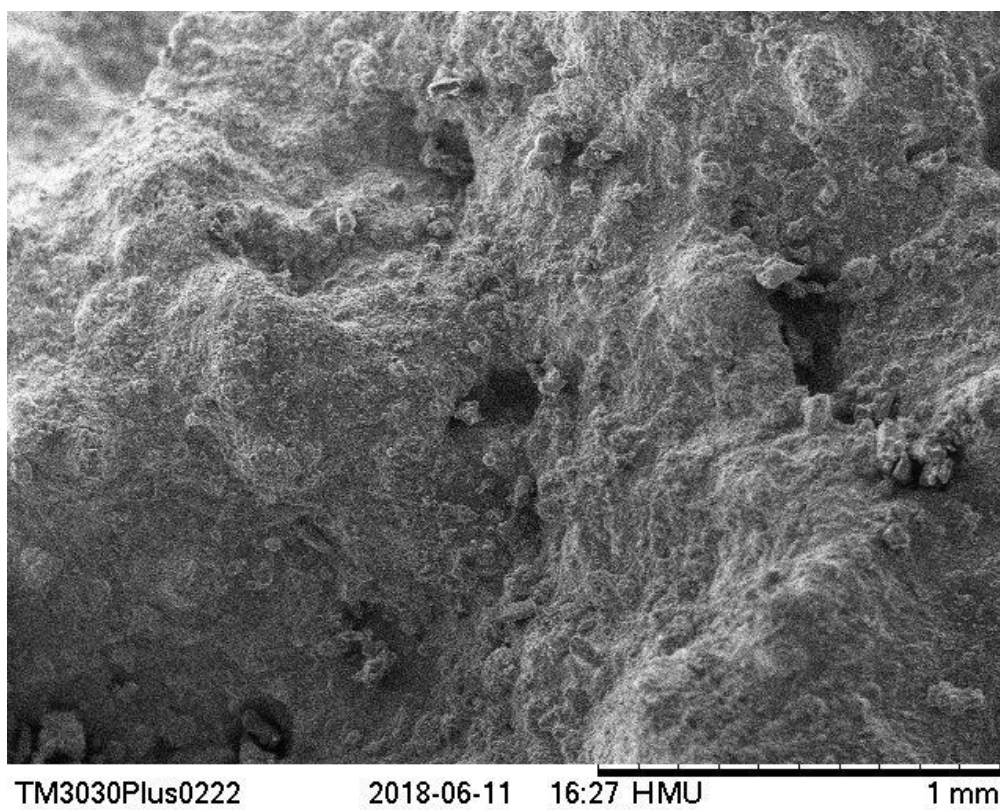
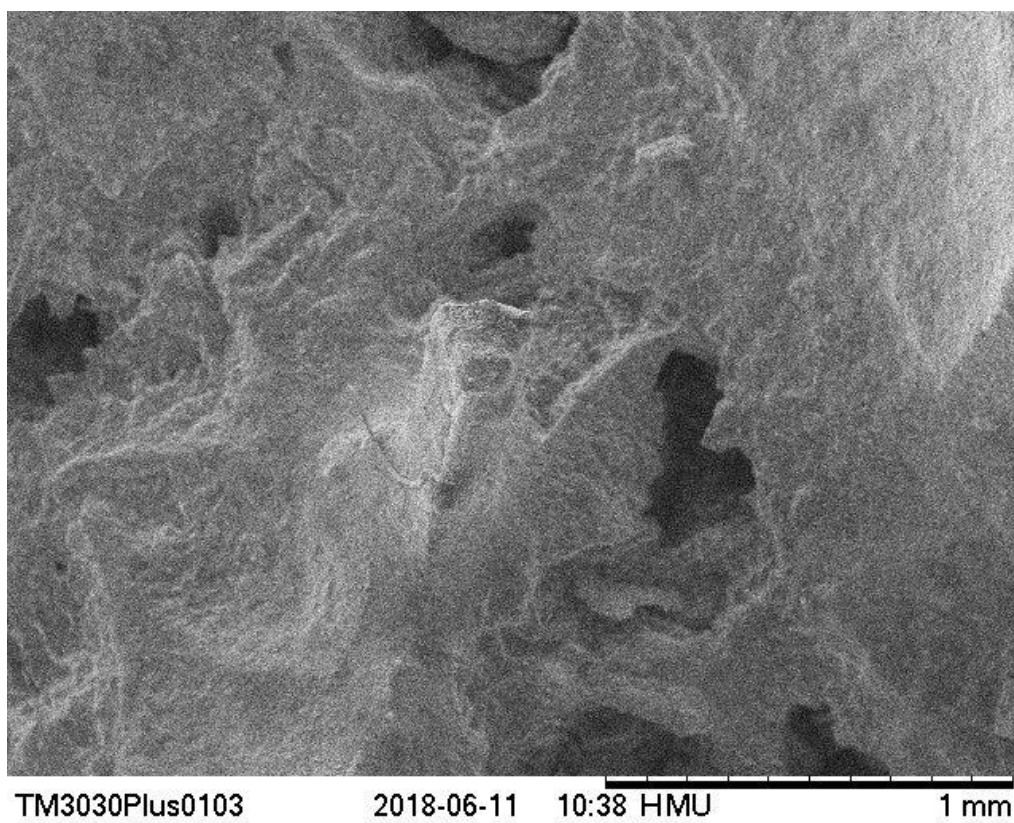


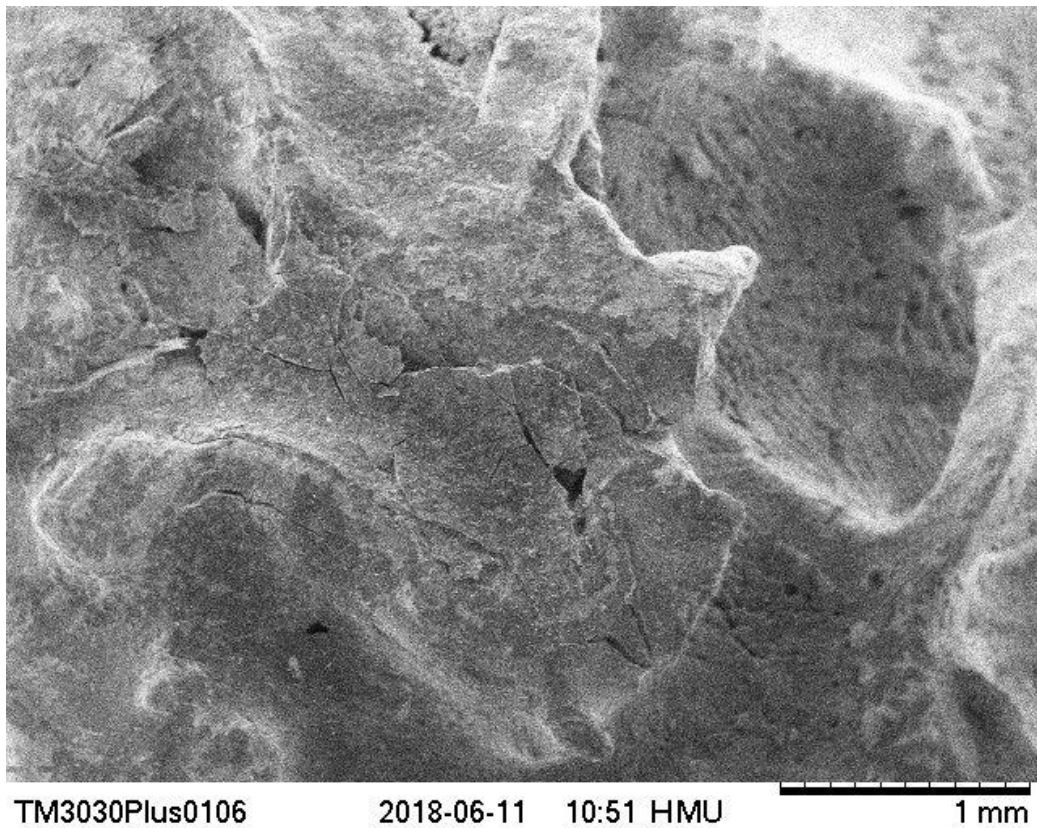
Fig. 2. Schematic of experimental test rig (a) section of test rig (b) layout of thermocouples. (Unit: mm)



(a)



(b)



(c)

Fig. 3. SEM images of HITEC salt/Al₂O₃ nanopowder with and without metal foam
(a) salt/2 wt. % Al₂O₃ nanopowder [26] (b) salt/nickel foam composite seeded with 2
wt. % Al₂O₃ nanopowder (c) salt/copper foam composite seeded with 2 wt.% Al₂O₃
nanopowder.

1

2

3

4

5

1

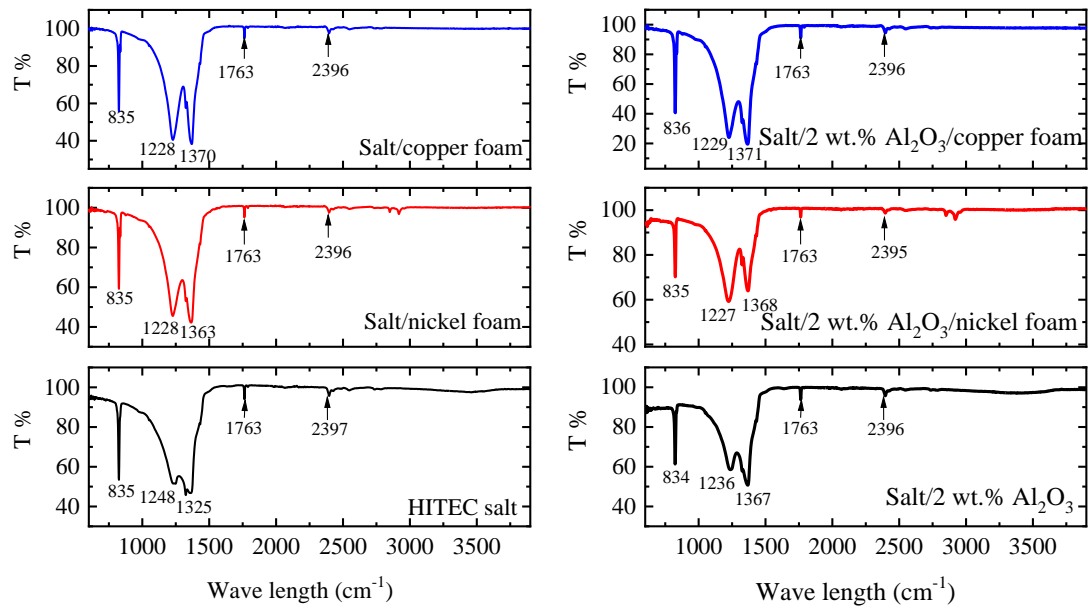


Fig. 4. FT-IR analyses of HITEC salt and composite PCMs.

2

3

4

5

6

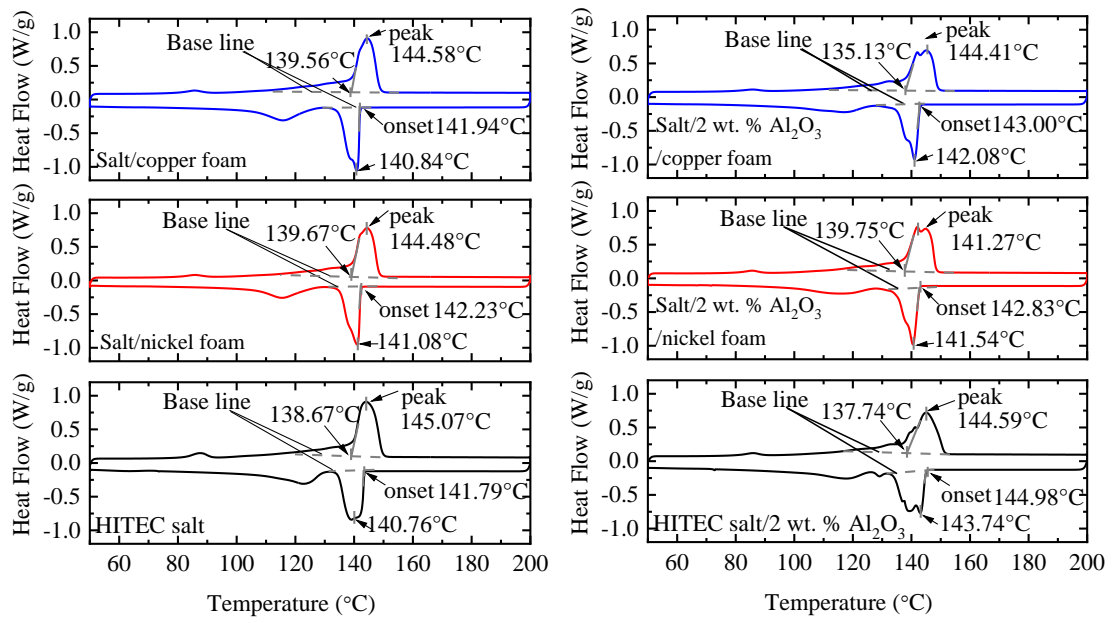


Fig. 5. DSC curves of HITEC salt and composite PCMs

1

2

3

4

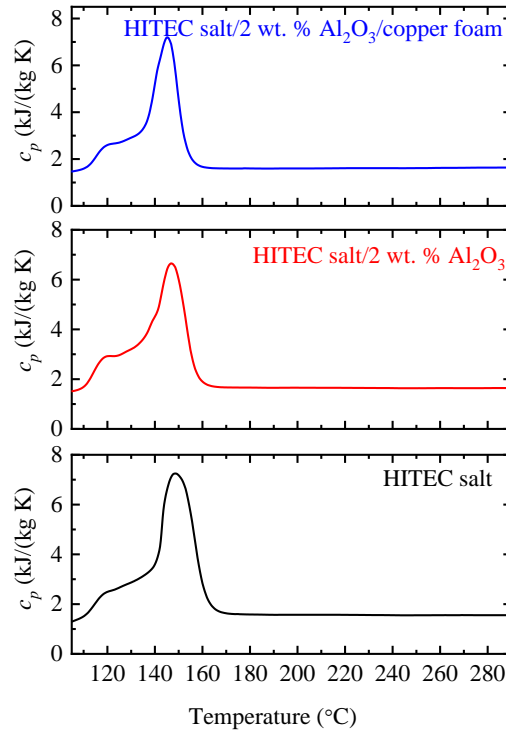
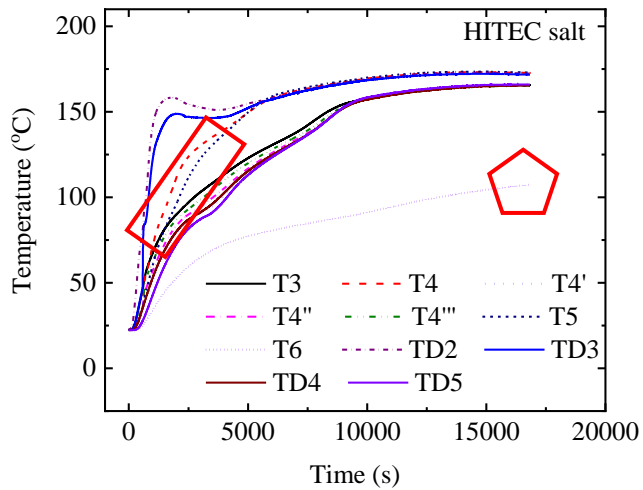


Fig. 6. Apparent specific heats of HITEC salt and composite PCMs.

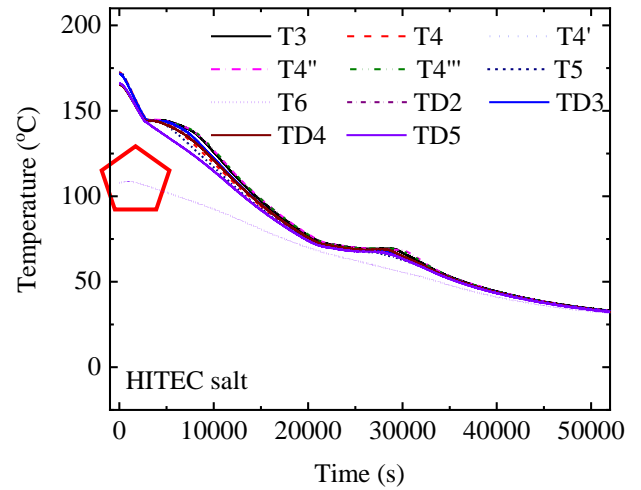
1

2

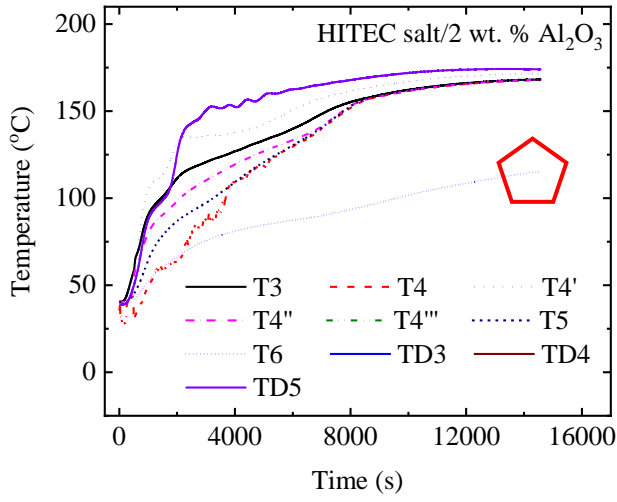
3



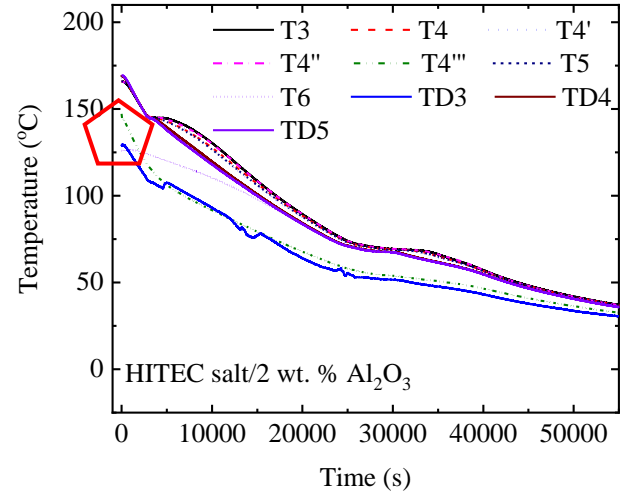
(a-I)



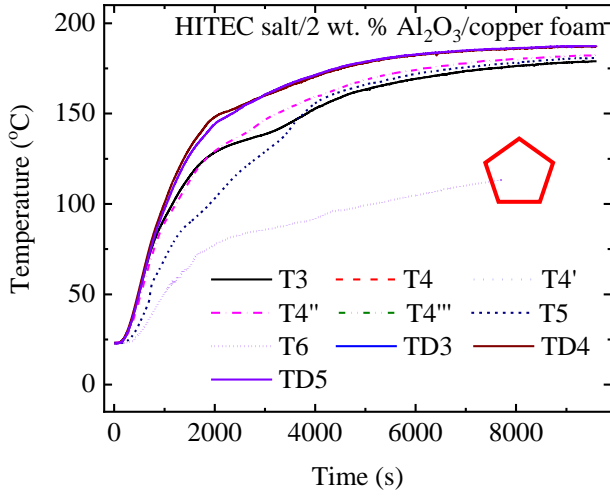
(b-I)



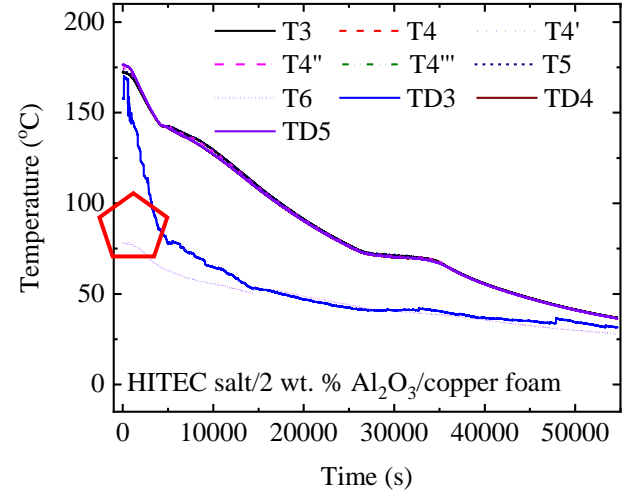
(a-II)



(b-II)



(a-III)

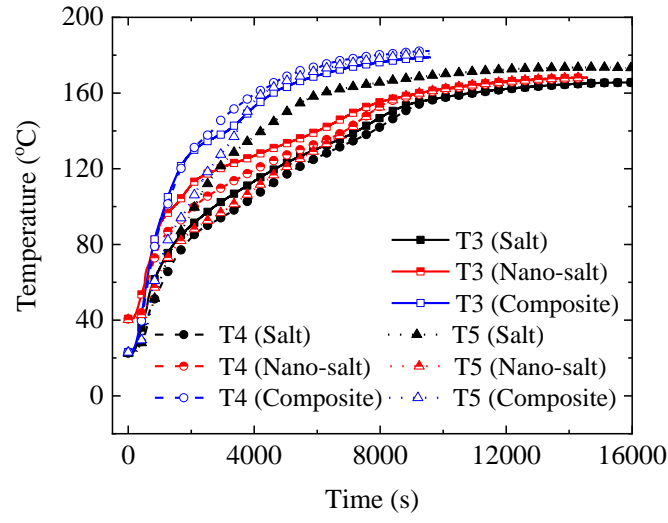


(b-III)

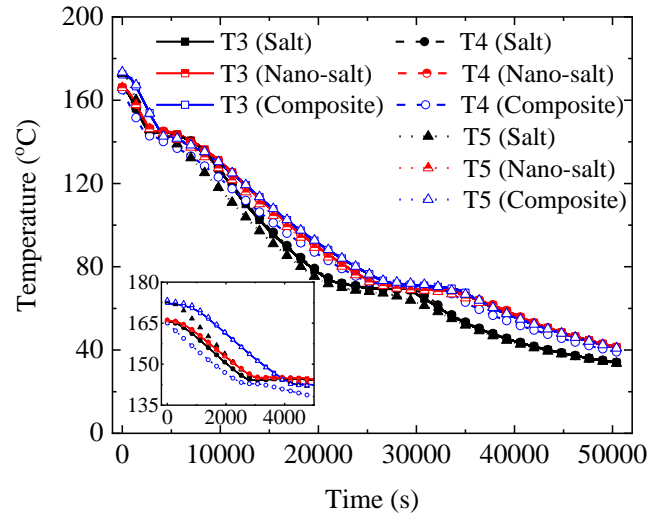
Fig. 7. Temperature evolutions and distributions of HITEC salt and composite PCMs ($T_{heating}=160\text{ }^{\circ}\text{C}$) (a) heat storage (b) heat retrieval. I, II, III marks represent HITEC salt, HITEC salt/2 wt. % Al_2O_3 nanopowder and HITEC salt/copper foam composite seeded with 2 wt. % Al_2O_3 nanopowder, respectively.

1

2



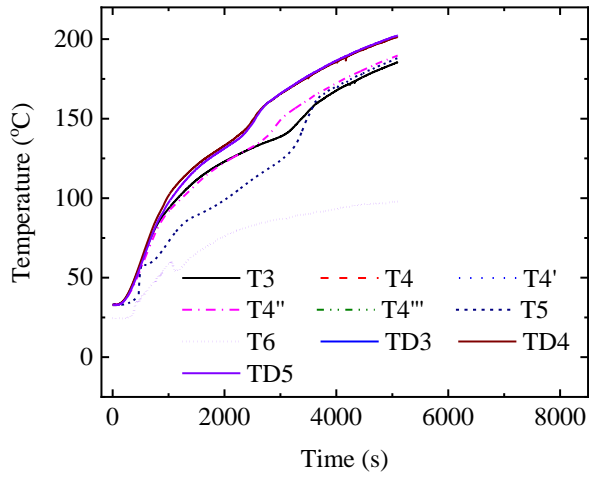
(a)



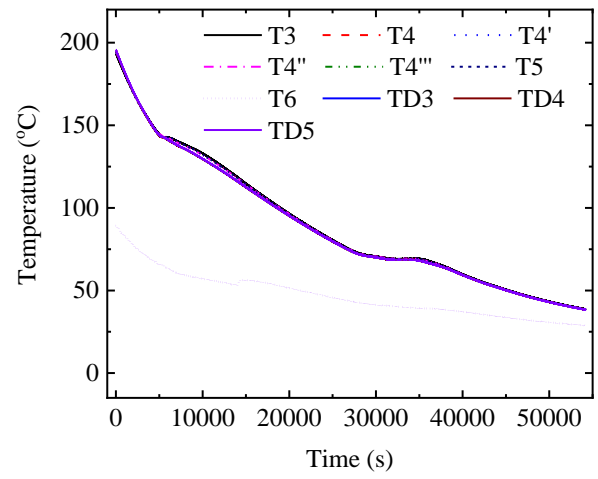
(b)

Fig. 8. Comparison of temperature evolutions and distributions of HITEC salt and composite PCMs ($T_{heating}=160$ °C) (a) heat storage (b) heat retrieval. The closed, half-open and open marks represent HITEC salt, HITEC salt/2 wt. % Al_2O_3 nanopowder and HITEC salt/copper foam composite seeded with 2 wt. % Al_2O_3 nanopowder, respectively.

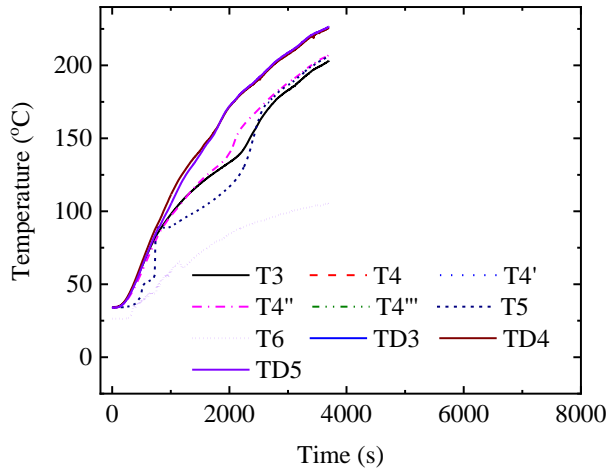
1



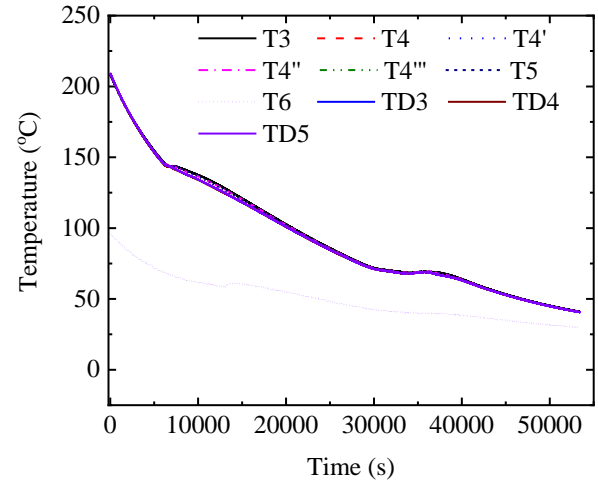
(a-I)



(a-II)



(b-I)



(b-II)

Fig. 9. Temperature evolutions and distributions of HITEC salt/copper foam composite seeded with 2 wt. % Al_2O_3 nanopowder at different heating temperatures (I: heat storage; II: heat retrieval)

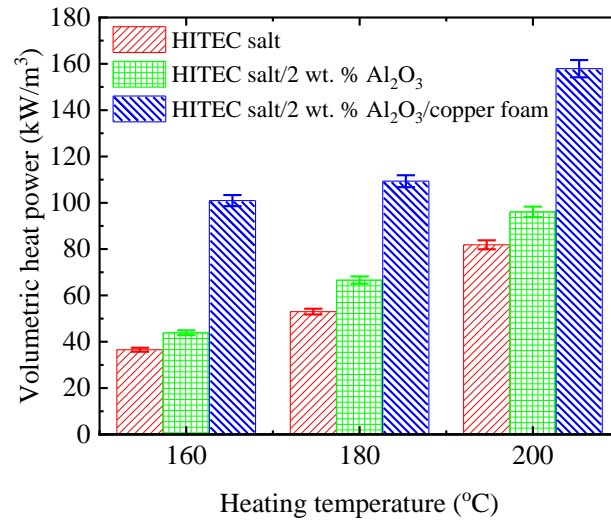
(a) 180 °C (b) 200 °C.

2

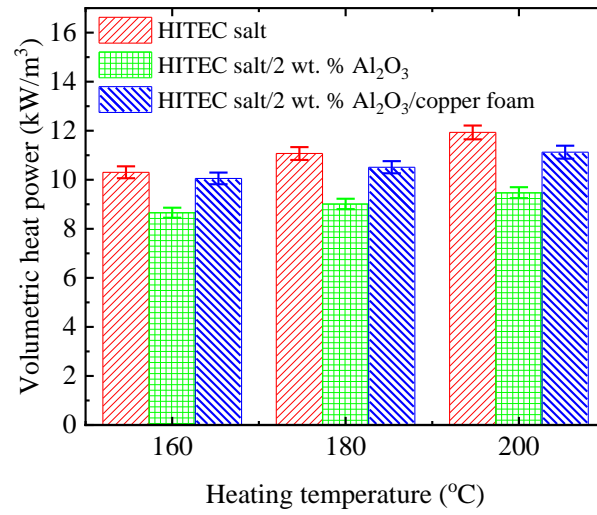
3

4

5



(a)



(b)

Fig. 10. Volumetric mean powers for HITEC salt and composite PCMs (a) heat storage (b) heat retrieval ($T_{end}=50$ °C).